Dynamic properties of ion guiding through nanocapillaries in an insulating polymer

N. Stolterfoht, R. Hellhammer, and D. Fink
Helmholtz-Zentrum Berlin für Materialien und Energie, Glienickerstrasse 100, D-14109 Berlin, Germany

B. Sulik and Z. Juhász
Institute of Nuclear Research (ATOMKI), H-4001 Debrecen, Hungary

E. Bodewits, H. M. Dang, and R. Hoekstra
KVI Atomic Physics, University of Groningen, 9747 AA Groningen, The Netherlands

(Received 7 November 2008; revised manuscript received 15 December 2008; published 3 February 2009)

We studied the dynamic properties of ion guiding through nanocapillaries in insulating polyethylene terephthalate. The angular distribution of the transmitted ions was measured as a function of the charge deposited on the sample surface, which is a measure of time. The time evolution of the angular transmission profiles was acquired for the capillary diameters of 200 and 400 nm. The tilt angle was varied from 0° to 6.5°. The transmission profiles appear as a superposition of essentially three localized peaks which exhibit significant changes in intensity as time varies. This observation provides evidence for the formation of temporary charge patches produced in the interior of the capillary besides the primary charge patch created in the entrance region.

DOI: 10.1103/PhysRevA.79.022901 PACS number(s): 61.85.+p, 34.50.Fa, 32.80.Fb

I. INTRODUCTION

In the past few years, the guided transmission of highly charged ions through nanocapillaries in insulating materials has attracted considerable attention. The guiding phenomenon involves charge-up effects that cause highly charged ions preserving their incident charge state during the transmission through the capillaries. The ions do not suffer close collisions with the capillary wall even when they are tilted with respect to the incident beam direction. This behavior is in contrast with results of the pioneering work with capillaries in metals [1,2].

Investigations of the ion guiding phenomenon in insulating materials have been started using capillaries in PET polymers [3–8]. Due to the increasing interest in this subject, several laboratories performed studies of capillary guiding with polyethylene terephthalate (PET) [9–11], SiO_2 [12], and Al_2O_3 [13–15]. Moreover, electrons were used as projectiles guided through capillaries in Al_2O_3 [16] and PET [17]. Tapered single-glass capillaries have been applied to produce submicrometer sized beams [18] that can be used for surface modification or to manipulate biological cells.

The capillary guiding phenomena can be understood in terms of a self-organizing process of charge deposition by the incident ions at the inner wall of the capillaries [3]. For a tilted foil the deposited charge in the entrance region increases until the electrostatic field is sufficiently high for a deflection of the ions towards the direction of the capillary exit. Then, the charge deposition reduces to an amount sufficient to maintain the field for the ion deflection to the exit. An increase of the incident current does not affect much the entrance charge patch, since the additional current flows away along the surface following a strongly nonlinear conductivity law [19].

The capability of insulating capillaries to guide ions is referred to as the *guiding power*. The fraction of transmitted ions at equilibrium generally decreases exponentially with the square of the tilt angle ψ. The guiding power can be quantified by the characteristic *guiding angle* ψ_c for which the normalized transmission fraction drops as $f(\psi_c)/f(0) = 1/e$ [19,20]. The guiding angle is a convenient parameter to characterize the guiding power which decisively depends on the material.

Monte Carlo simulations [23,24] have explicitly shown that most of the deposited charge is located near the entrance region. Additional weaker patches may temporarily be produced after the formation of the first patch. The temporary patches play a significant role in the guiding process during the pre-equilibrium period. They change their position and strength so that dynamic properties of the ion guiding become important. Experimentally, the dynamic effects can be observed by measuring transmission profiles as a function of time. Experimental studies concerned with the dynamic aspects of the capillary guiding [19,25,26], have shown that the formation of temporary patches can be revealed by studying angular shifts of the transmission profiles.

In the present work, we investigate the dynamic properties of 3 keV Ne^{7+} ion guiding through capillaries in insulating PET. Preliminary results of this work have been reported elsewhere [21]. The angular transmission profiles exhibit three distinct peaks whose positions are rather stable. The peak intensities strongly change in a characteristic manner resulting in a damped oscillation of the mean emission angle. At equilibrium, this angle reaches a value equal to the tilt angle of the capillary. The observations are interpreted by means of temporary charge patches formed inside the capillaries.

II. EXPERIMENTAL METHOD

The experiments were conducted in an ultrahigh vacuum chamber mounted at the 14 GHz Electron Cyclotron Resonance (ECR) ion source of the ZERNIKE-LEIF facility at

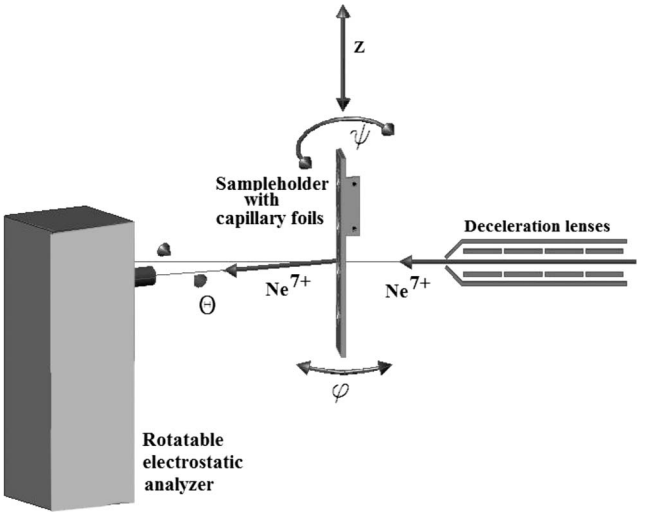

FIG. 1. Experimental setup used in the experiments. Ions from the ECR ion source are decelerated in a lens system and directed on the capillary sample mounted on a target ladder. The target foil can be tilted by the angles ψ and φ and shifted perpendicular to the plane in the x direction and the z direction as indicated. The transmitted ions are measured by an electrostatic analyzer rotated by the angle θ.

the KVI Groningen (Netherlands) [27]. The experimental setup is shown in Fig. 1. For the present experiments the base pressure in the chamber was some 10^{-8} mbar. The chamber was operated on high voltage to allow for the deceleration of the incident Ne^{7+} ions from 49 to 3 keV along a set of deceleration lenses. The current was varied within the range of 10–1000 pA. The beam was collimated to a diameter of 1 mm with a divergence better than 0.2° full width at half maximum (FWHM).

The capillary foils were mounted on a target ladder that could hold four samples. The target ladder was fixed at a goniometer, which allowed for tilting the capillaries relative to the incident beam in two directions specified by the angles ψ and φ (Fig. 1). The tilt angle ψ was varied to change the angle between the incident beam and the capillary axis. The azimuthal angle φ was kept constant after its zero value was determined. The PET target foils were mounted on circular frames with an inner diameter of 7 mm. The target could be moved by the goniometer in two dimensions (up-down and left-right) with respect to the incident ion beam. Thus the ion beam could be positioned at different spots within the target area (of 7 mm in diameter). With the beam diameter of 1 mm FWHM the ion beam could be located at five well-separated spots. One beam spot was used for the adjustment of the zero position of the angles ψ and ϕ with an accuracy of $\pm 0.2°$. The remaining four spots were used for the experiments. Hence the results described below for each tilt angle and diameter were obtained with fresh capillaries, which have not been irradiated since the last beam time of about three months ago.

The ions transmitted through the capillaries were measured using an electrostatic 180° analyzer, which was rotated by the angle θ in the same plane as the tilt angle ψ. The quadratic entrance slit of the analyzer has an opening of 0.4 mm and was located 75 mm away from the target position. Hence the angular resolution of the analyzer is obtained as 0.2° FWHM. With the analyzer a Gaussian-like angular profile with a FWHM of 0.6° was measured for the direct incident beam (without the capillary target). This width is a composition of the beam width, its divergence, and the angular resolution of the analyzer.

The energy resolution of the analyzer was 0.5%, which was high enough to separate the charge states of the transmitted ions. In fact, the energy resolution was significantly higher than required for the present experiments. With this high resolution the analyzer reading was sensitive to energy shifts of the incident beam due to fluctuations of the plasma potential in the ECR source. Therefore during the experiments care was taken to adjust the analyzer settings for small temporal changes of the plasma potential.

For the present experiments, two PET samples with the capillary density of 4×10^6 cm^{-2} were used as prepared at the Ionenstrahllabor (ISL) in Berlin [22]. The thickness of the samples was 12 μm. The two samples differ in the capillary diameters which were 200 and 400 nm. The density of the capillaries implies a geometric opening of 0.12% and 0.48%, respectively. The mean distance was about 5 μm between neighboring capillaries. It is evident that an overlap of adjacent capillaries is unlikely to happen. Gold was evaporated under 30° on the front and the back side of the PET foil forming a film of ~20 nm thickness to avoid a macroscopic charge up of the sample surfaces.

Care was taken to minimize the nonparallelism of the capillaries. The angular spread of the capillary inclination was estimated to be $\lesssim 0.2°$ FWHM which was significantly smaller than the aspect angles of 1° and 2°, respectively. This small FWHM is a decisive condition for the present experiments where the time evolution of angular profiles were measured for the transmitted ions. When the capillaries are not parallel, the ions are first transmitted at angles smaller than the capillary tilt angle, because the ion transmission is favored through nonparallel capillaries with smaller tilt angles. This effect has previously been observed [6] with nonparallel capillaries (FWHM of 2°) where ions were first emitted at 0° although the capillary sample was tilted by 5°.

III. EXPERIMENTAL RESULTS

In the following, we focus our attention on Ne^{7+} ions, whose incident charge state was preserved during the passage through the capillary. The left columns of Figs. 2 and 3 contain a series of transmission profiles for capillary diameters of 200 and 400 nm, respectively. A transmission profile is an angular distribution $dY(\theta,\phi)/d\Omega$ of Ne^{7+} ions transmitted through the capillaries as a function of the observation (or emission) angle θ with $\phi=0$. The angles θ and ϕ are defined relative to the incident beam direction so that $d\Omega = d\theta d\phi$. For the examples shown in Figs. 2 and 3 the tilt angle of $\psi=5°$ was chosen.

Each transmission profile is normalized to an integrated current of $Q_d=1$ nC, i.e., the beam charge deposited on the front surface of the PET target foil. For a given incident beam current the deposited charge is a measure of time. Each

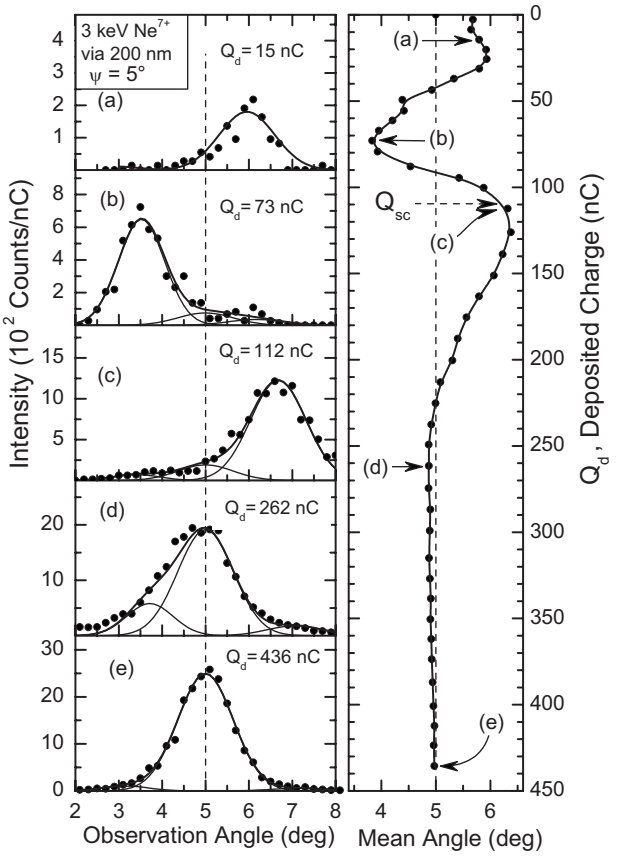

FIG. 2. Transmission profiles and mean angle for 3 keV Ne^{7+} ions transmitted through capillaries of 200 nm in diameter. In the left column the profiles are shown for increasing charge Q_d deposited at the target. The profiles are fitted by a sum of three Gauss functions given as solid lines. The right column shows the related mean emission angle. Note that the labels (a)–(e) in the left column correspond to those given in the right column. The arrow labeled "Q_{sc}" indicate the charge for which ~63% of the equilibrium intensity of the transmitted ions is reached.

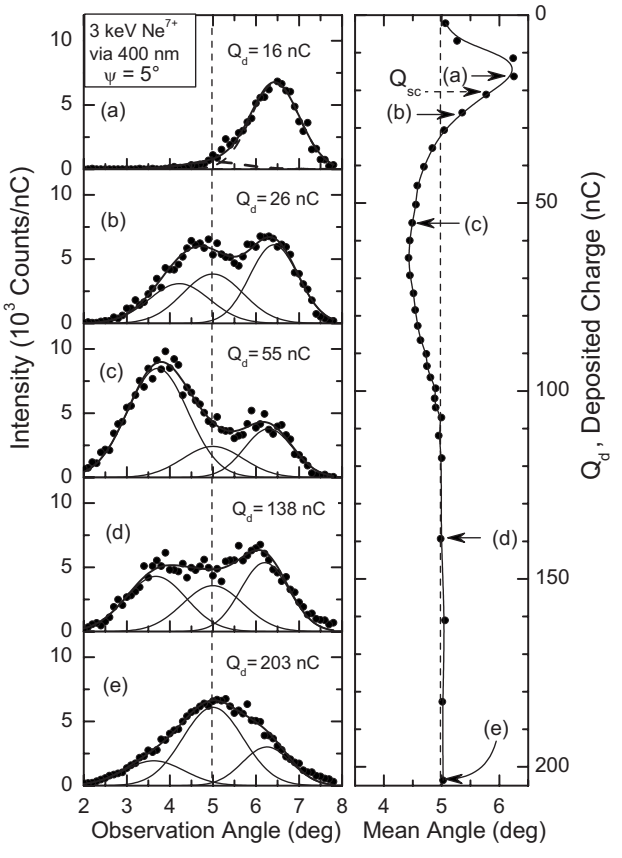

FIG. 3. Transmission profiles and mean angle for 3 keV Ne^{7+} ions transmitted through capillaries of 400 nm in diameter. Further caption text as in Fig. 2.

graph indicates the total charge Q_d collected till the instant when the profile is measured. The charge deposited during a scan of a profile is smaller than the charge collected between two successive scans.

The transmission profiles exhibit three peak structures, whose positions appear to be rather constant. Hence we fitted the experimental data by a superposition of three Gauss functions. The location of the central peak was assumed to be equal to the tilt angle of 5° and it was kept constant. Also, the FWHM's of the individual peaks were assumed to be constant being equal to 1.5° and 1.65° for 200 and 400 nm capillaries, respectively. However, in contrast to our preliminary analysis [21], the positions of the first and third peak were now treated as adjustable parameters, as well as the all peak heights. The fits exhibit that the positions of the first and third peaks were rather constant, i.e., the centroid values were found to be at $3.7° \pm 0.2°$ and $6.4° \pm 0.3°$, respectively. Thus these peaks are displaced with respect to the tilt angle of 5° by ~1.4°. For 200 nm capillaries this value is larger than the aspect angle of 1°.

For the 200 nm capillaries (Fig. 2) the third peak appears at the observation angle 6° within a charge deposition of less than 75 nC [see Figs. 2(a) and 2(b)]. It readily moves to its final position near 6.5° as the charge deposition exceeds 75 nC. For the 400 nm capillaries the third peak initially appears at the observation angle of 6.5° [see Figs. 3(a) and 3(b)] and it moves to its final position near 6.3° as the charge deposition exceeds 75 nC. Hence an individual peak may move in the beginning, but its position becomes stable after some charge deposition.

From the transmission profiles it is seen that the individual peaks change significantly in intensity with increasing charge deposition. Consequently, the mean values of the emission angle are varying as shown in the right columns of Figs. 2 and 3. The mean emission angle is obtained by the well-known expression $\int \theta(dY/d\Omega)d\theta / \int (dY/d\Omega)d\theta$. The results exhibit oscillatory displacements within the range from 3.8° to 6.3° for 200 nm and from 4.2° to 6.3° for 400 nm capillaries. This indicates that at the extremes (reversal points) either the first or third peak dominates. In between the reversal points the profiles appear as a superposition of three peaks of similar intensity [in particular see Figs. 3(b) and 3(d)]. Note that the labels (a) to (e) in the left column correspond to the same labels in the right column.

When the charge deposition progresses, the oscillations are damped. For the 400 nm capillaries the damping is stronger than that for 200 nm and hence more oscillations are visible for the smaller diameter. Altogether, for 200 nm the mean emission angle exhibits four extremes (minima and

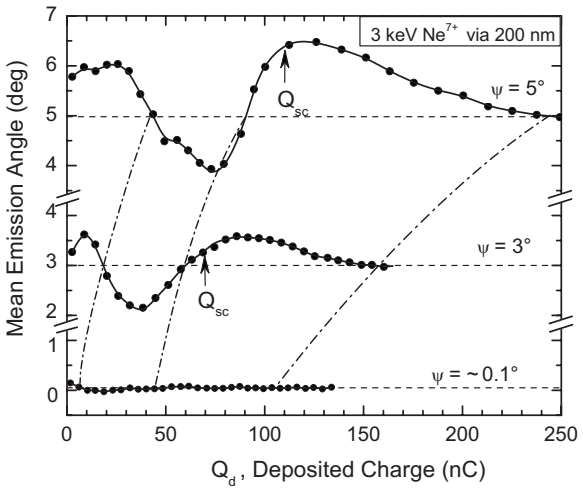

FIG. 4. Mean emission angle of the transmitted Ne^{7+} ions for capillary tilt angles of 0°, 3°, and 5°. The dashed lines are drawn to guide the eye along the nodes of the mean angles. The arrows labeled "Q_{sc}" indicate the charge for which 63% of the equilibrium ion intensity is reached.

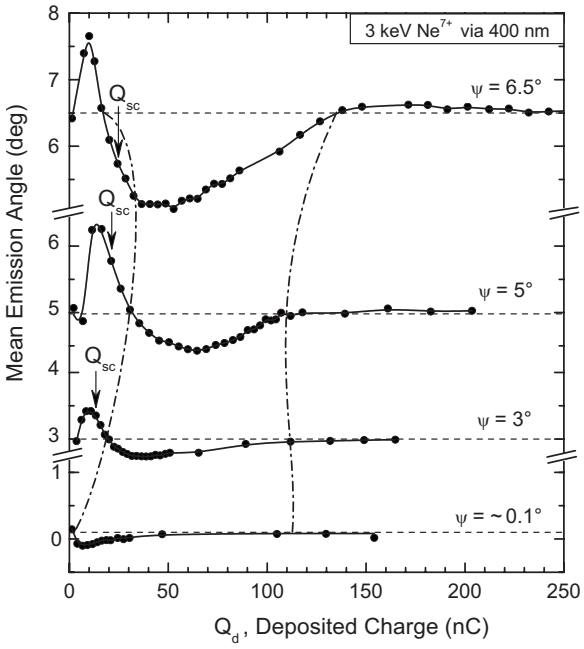

FIG. 5. Mean emission angle of the transmitted Ne^{7+} ions for capillary tilt angles of 0°, 3°, 5°, and 6.5°. The further text as in Fig. 4.

maxima) resulting from its oscillation, whereas for the 400 nm capillaries only three extremes are visible. After considerable damping the mean emission angles do not change any more. Finally, the mean angles coincides with the tilt angle of 5° and the central peaks become dominant. For the 400 nm results (Fig. 3) we note that the equilibrium may not be fully reached, i.e., the side peaks may still decrease with respect to the center peak.

In Fig. 4 the mean angles of the 200 nm capillaries are compared for different tilt angles. It is seen that for 3° and 5° the oscillatory structures are similar. In fact, the 0° curve also shows (the same) tiny oscillations, which suggest that the capillaries are tilted by the small amount of $\lesssim 0.1°$. This value lies within the experimental uncertainties of the tilt angle setting. To guide the eye, the corresponding zero points (nodes) of the mean emission angles are connected by dashed lines as shown in Fig. 4. It is seen that the corresponding nodes are shifted to higher values of the deposited charge as the tilt angle increases from 0° to 5°.

In Fig. 5 the mean angles of the 400 nm capillaries are plotted for 0°, 3°, 5°, and 6.5°. The oscillation for 400 nm look similar as those for 200 nm although less extremes are visible. Also, the first node is shifted to higher values of the deposited charge as the tilt angle increases from 0° to 5°, while the 6.5° node turns back to lower charges. Moreover, the second node is shifted to higher charge values also for 6.5°.

To obtain more information about the differences between the 200 and 400 nm capillaries and the shift of the nodes we compare the evolution of the emission angle with that of the total ion yield Y, which is obtained by integration of the transmission profiles [represented by the differential yield $dY(\theta,\phi)/d\Omega$]. Since the angular measurements were restricted to one dimension, the integration could be performed only with respect to the angle θ. The integration over ϕ was replaced in an approximation by the multiplication with the constant angle $\Delta\phi$, which was assumed to be equal to the corresponding equilibrium angle $\Delta\theta$.

As shown previously [19] the charge evolution of the total ion yield can be approximated by the exponential function

$$Y(Q_d) = Y_0\left[1 - \exp\left(-\frac{Q_d - Q_s}{Q_c}\right)\right], \tag{1}$$

where Q_s is a threshold value and Q_c is a characteristic charge for which $\lesssim 63\%$ of the equilibrium value Y_0 is reached. Since the equilibrium is approached asymptotically, it is not possible to define a point where it is fully reached. Considering the values of 80–90 % (corresponding to the experimental uncertainties of $\lesssim 20\%$) one may assume that the equilibrium value is reached at about 3 times Q_c.

We determined the values of Q_s and Q_c by fitting the corresponding total ion yield with the expression in Eq. (1). In Fig. 6 the fit functions are shown in conjunction with the numerical values of Q_s and Q_c. It is seen that the sum $Q_{sc} = Q_s + Q_c$ increases with increasing tilt angle. (Note that $Q_{sc} \approx Q_c$ since $Q_s \ll Q_c$.) Also, Q_{sc} is significantly larger for 200 nm capillaries than that for 400 nm. This may be attributed to the fact that more charge must be deposited on the sample surface in order to introduce the same charge into the 200 nm capillaries than into the 400 nm capillaries, as discussed in more detail further below.

In Fig. 6 it is seen that the experimental data overshoot the corresponding fitting functions in the range of 25–50 nC. The overshot is clearly visible in the results for 400 nm capillaries in the right hand column, but it can also be seen in the left hand column. The position of the overshot varies slightly with the tilt angle, similarly as Q_{sc}. It appears that the transmitted ion yield also exhibits some oscillatory behavior.

Let us now focus on the angular oscillations for the different tilt angles. In Figs. 4 and 5 the charge Q_{sc} is marked

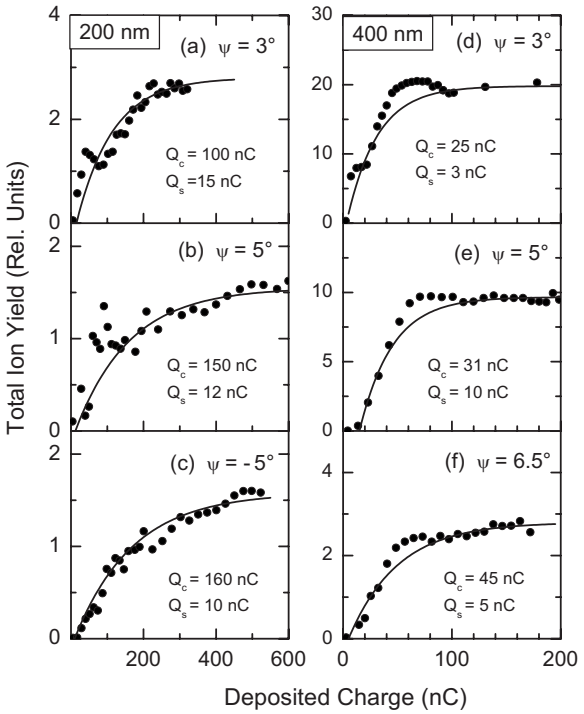

FIG. 6. Total ion yield Y of Ne^{7+} transmitted through capillaries with diameter of 200 nm (left hand column) and 400 nm (right hand column). The tilt angles ψ are indicated in each graph. The experimental data given as circles are fitted by Eq. (1). The results are shown as lines for which the fit values Q_s and Q_c are also given in the corresponding graphs.

by arrows labeled "Q_{sc}." It is seen that the arrows are shifted in the same sense as the corresponding nodes of the mean emission angle. Moreover, the arrows reveal that the main oscillations occur before reaching the equilibrium. After the equilibrium is approached within 10%, smaller damped oscillations are still present. This shows that the oscillations of the mean angle and the evolutions of the corresponding ion intensity are closely related.

Next, we consider the differences between the results obtained with 200 and 400 nm capillaries (Figs. 4 and 5). With a tilt angle of 5° the characteristic charges are determined to be $Q_{sc}=110$ and 20 nC for 200 and 400 nm capillaries, respectively (Fig. 6). These charge values show that within the deposition of $\sim 3Q_{sc}$ a total number of 3 and 2 extremes are covered for the 200 and 400 nm capillaries, respectively. Hence the number of oscillations is larger for the 200 nm capillaries.

We recall that Q_{sc} is a charge deposited at the surface of the capillary sample. To calculate the charge that is inserted into the capillaries, we have to take into account the geometric capillary openings. The opening of the capillaries increases by the factor of 4, i.e., the number of inserted elementary charges are $105e$ and $420e$ per nC for the capillary diameters of 200 and 400 nm, respectively. Thus with respect to the charge deposition within the capillary, the present results show that the mean angle for the 200 nm capillaries oscillates faster than that for 400 nm. Hence there are obvious differences between the results of the two capillary diameters. We shall return to this point in the following discussion

IV. DISCUSSION AND CONCLUSIONS

In the present analysis, the time evolution of transmission profiles is studied for 3 keV Ne^{7+} ions using PET capillaries with a diameter of 200 and 400 nm. The profiles exhibit oscillatory displacements of the mean emission angle, which are similar for different tilt angles. A repetition of the measurements revealed that the oscillations and peak structures in the transmission profiles are reproducible. Also, the oscillations are similar for the different capillary diameters. Hence we may state that the peak structures and the oscillations are general phenomena for the present PET capillaries.

We attribute the oscillatory behavior to temporary charge patches formed inside the capillaries. This conclusion is based on the finding that at the reversal points, the emission angles α are found to be negative or to exceed the aspect angle of 1° for 200 nm capillaries. Recall that the observation angle θ is defined relative to the incident beam direction, while the emission angle $\alpha=\theta-\psi$ is defined relative to the capillary axis.

Let us first consider ion transmission through the 200 nm capillaries. In Fig. 7 a tentative scenario of the patch formation is shown. The ions incident with an angle of 5° produce the relatively stable charge patch in the entrance region of the capillary. When sufficient charge is deposited in the entrance patch, the ions are deflected to the exit of the capillary. In fact, the ions are temporarily moving from one corner in the entrance region to the opposite corner of the exit region.

Hence relative to capillary axis the ions leave the capillary under the emission angle of $\alpha \approx 1°$ equal to the aspect angle of the 200 nm capillaries. Thus it follows that the emission angle of ~6° relative to the incident beam direction is larger than the tilt angle [Fig. 7(a)]. As the entrance charge patch further increases the ions are directed to the opposite wall near the exit region whereby a secondary charge patch is produced. Thus the ions are deflected so that the emission angle relative to the incident beam direction becomes smaller

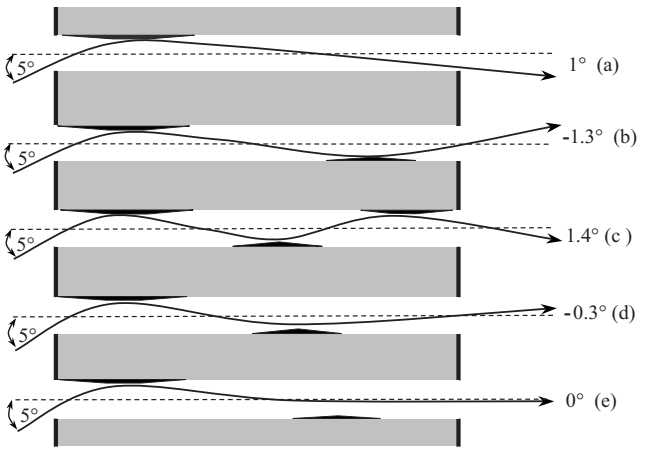

FIG. 7. Tentative scenario of temporary patches produced in the interior of the 200 nm capillaries. The labels (a)–(e) correspond to those given in Fig. 2. The dominant rather stable patch is created in the entrance region. Further patches are temporarily produced in the interior of the capillary. Note that for graphical reason the aspect ratio is strongly reduced and thus angles are enhanced. (Details are given in the text.)

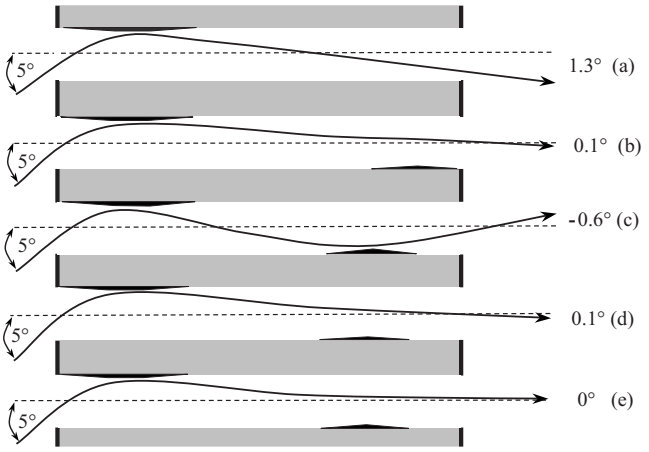

FIG. 8. Tentative scenario of temporary patches produced in the interior of the 400 nm capillaries. The labels (a)–(e) correspond to those given in Fig. 3. Further figure caption as in Fig. 7.

than the tilt angle [Fig. 7(b)]. When the charge in the entrance patch further increases the secondary patch moves into the interior of the capillary and a tertiary patch is produced. Then, the ions are deflected into the same direction as in the first stage (a) but with an angle larger than the aspect angle [Fig. 7(c)]. After formation of the tertiary patch, the charge deposition is reduced and the deflection by the entrance patch becomes weaker. Also, the tertiary patch loses significance [Fig. 7(d)]. Finally, the ions are guided along the capillary axis by the remaining charge in a small secondary patch near the capillary exit [Fig. 7(e)].

Next, we consider the possible scenario for the 400 nm capillaries. In this case, the aspect angle is 2° and the ions can leave the capillary under larger angles without forming a temporary patch. At the beginning, the ions are deflected only by the entrance patch and leave the capillaries under the mean angles of $\lesssim 1.3°$ [Fig. 8(a)]. As the entrance charge patch further increases, a secondary charge patch is formed at the opposite wall. The angle relative to the incident beam direction becomes smaller, i.e., the ions are leaving the capillary under the angle of 0.1° as shown in Fig. 8(b). When the secondary patch increases, the ions are deflected to a negative angle of −0.6° so that the ions are leaving the capillary with an angle smaller than the tilt angle [Fig. 8(b)]. Now, the ions have to leave the entrance patch under a relatively large angle of $\sim 2°$ which may lower the charge deposition near the entrance. Thus the ion deflection is reduced and the tertiary patch is not likely to be produced. Hence the case depicted in Fig. 7(c) does not occur. Rather the situation becomes similar to Fig. 8(b) with an emission angle slightly larger than the tilt angle because of the weak deflection in the secondary patch [Fig. 8(d)]. Finally, the ions are guided along the capillary axis by the remaining charge of the secondary patch as shown in Fig. 8(e).

Comparing the different capillary diameters we recall that less charge patches are produced for the 400 nm capillaries. Also we note that in the 200 nm capillaries the formation of the secondary patch needs a smaller emission angle from the entrance patch than in the 400 nm capillaries, i.e., about 1° in comparison with 2°. Hence the secondary patch is expected to be formed more rapidly. Thus it appears plausible that for 200 nm capillaries the mean angle oscillates more rapidly as noted above.

Recently, the formation of temporary patches has experimentally been studied [25,26] yielding results which are in qualitative agreement with the present data. Moreover, the essential features of the simulations [23,24] are in agreement with the present experimental results. The temporary patches are important in the pre-equilibrium period, whereas at equilibrium the ions are transmitted predominantly along the capillary axis. However, some details of the temporary patch production are different from the present results. In fact, discrepancies are expected for capillaries of different material and aspect ratio.

Kanai *et al.* [26] noted that their number of charge patches differ from those considered by Skog *et al.* [25] and attributed this finding to differences in the capillary aspect ratios used in the two experiments. Similar observations were made in the present studies where the number of patches differ for the capillaries of 200 and 400 nm. Moreover, differences occur in the oscillatory behavior of the transmitted ions. In the present data (and in most results by Kanai *et al.* [26]) the transmission starts at an angle close to the tilt angle and moves rapidly to larger angles (Figs. 2 and 3). This finding is in contrast to the work by Skog *et al.* [25] wherein the ion transmission starts at angles smaller than the tilt angle. The latter unexpected observation was attributed to the fast creation of a temporary patch at the capillary exit. On the other hand, we recall the possibility of nonparallelism capillaries, which favor the ion transmission at smaller angles.

Finally, we focus our attention on the transmission profiles which are composed of three distinct peaks of comparable intensity. The occurrence of peaks with rather fixed positions may be counterintuitive, since the transmission profile is continuously moving with an oscillatory behavior. However, the distinct peaks were identified in several measurements after changing the tilt angle and the capillary diameter. Recall that the peak positions (except the center peak) were treated as variable fit parameters. We found time intervals wherein the peak locations remain fixed and cases where they vary somewhat with time. One is tempted to attribute each peak to a certain charge patch produced in the capillary. However, such an assignment has its limits and needs further studies.

We suggest that the distinct peaks are due to groups of trajectories entering the capillary at different distances from the entrance patch. Ions in one group of trajectories may be guided directly to the capillary exit whereas ions of another group may be deflected by a temporary patch. In fact, the deflection of different groups of trajectories involving temporary patches and the formation of two separated peaks in a transmission profile have theoretically been demonstrated for a single capillary [24]. It should be added that we also tried to fit the measured profiles with two Gauss functions of variable positions and widths. Such fit is possible, but the reproduction of the experiment was not satisfactory in specific cases [e.g., see the profiles in Figs. 3(b) and 3(d)].

In conclusion, we observed pronounced oscillations in the time evolution of transmission profiles for ions passing through nanocapillaries. Unexpectedly, the profiles were

found to be composed of distinct peaks whose origin needs further experimental and theoretical work. Emphasis is given to studies of capillaries with different diameters. In particular, the formation of different numbers of temporary patches for capillaries of different diameters and aspect ratios appears to be an interesting observation that deserves further attention. Moreover, clarifying studies are required to investigate the influence of effects due to statistical fluctuation in surface properties between neighboring capillaries.

ACKNOWLEDGMENTS

We are indebted to Yasuyuki Kanai for stimulating discussions. B.S. and Z.J. were supported by the Hungarian National Science Foundation OTKA (Grants No. K73703 and No. PD050000). This experiment was performed at the distributed LEIF-Infrastructure at ZERNIKE-LEIF. The work was financially supported by the European Network ITSLEIF RII3-026015

[1] S. Ninomiya, Y. Yamazaki, F. Koike, H. Masuda, T. Azuma, K. Komaki, K. Kuroki, and M. Sekiguchi, Phys. Rev. Lett. **78**, 4557 (1997).
[2] K. Tökési, L. Wirtz, C. Lemell, and J. Burgdörfer, Phys. Rev. A **61**, 020901(R) (2000).
[3] N. Stolterfoht, J. H. Bremer, V. Hoffmann, R. Hellhammer, D. Fink, A. Petrov, and B. Sulik, Phys. Rev. Lett. **88**, 133201 (2002).
[4] N. Stolterfoht, V. Hoffmann, R. Hellhammer, D. Fink, A. Petrov, Z. D. Pešić, and B. Sulik, Nucl. Instrum. Methods Phys. Res. B **203**, 246 (2003).
[5] N. Stolterfoht, R. Hellhammer, Z. D. Pešić, V. Hoffmann, J. Bundesmann, A. Petrov, D. Fink, and B. Sulik, Vacuum **73**, 31 (2004).
[6] N. Stolterfoht, R. Hellhammer, Z. D. Pešić, V. Hoffmann, J. Bundesmann, A. Petrov, D. Fink, B. Sulik, M. Shah, K. Dunn, J. Pedregosa, and R. W. McCullough, Nucl. Instrum. Methods Phys. Res. B **225**, 169 (2004).
[7] R. Hellhammer, P. Sobocinski, Z. D. Pešić, D. Fink, J. Bundesmann, B. Sulik, and N. Stolterfoht, Nucl. Instrum. Methods Phys. Res. B **232**, 235 (2005).
[8] R. Hellhammer, P. Sobocinski, Z. D. Pešić, D. Fink, J. Bundesmann, B. Sulik, and N. Stolterfoht, Nucl. Instrum. Methods Phys. Res. B **233**, 213 (2005).
[9] Gy. Víkor, R. R. Kumar, Z. Pešić, N. Stolterfoht, and R. Schuch, Nucl. Instrum. Methods Phys. Res. B **233**, 218 (2005).
[10] Y. Kanai, M. Hoshino, T. Kambara, T. Ikeda, R. Hellhammer, N. Stolterfoht, and Y. Yamazaki, Nucl. Instrum. Methods Phys. Res. B **258**, 155 (2007).
[11] M. Fürsatz, W. Meissl, S. Pleschko, I. C. Gebeshuber, N. Stolterfoht, H. P. Winter, and F. Aumayr, J. Phys.: Conf. Ser. **58**, 319 (2007).
[12] M. B. Sahana, P. Skog, G. Víkor, R. T. Rajendra Kumar, and R. Schuch, Phys. Rev. A **73**, 040901(R) (2006).
[13] S. Mátéfi-Tempfli, M. Mátéfi-Tempfli, L. Piraux, Z. Juhász, S. Biri, É. Fekete, I. Iván, F. Gáll, B. Sulik, G. Víkor, J. Pálinkás, and N. Stolterfoht, Nanotechnology **17**, 1 (2006).
[14] H. F. Krause, C. R. Vane, F. W. Meyer, and H. M. Christen, J. Phys.: Conf. Ser. **58**, 323 (2007).
[15] P. Skog, I. L. Soroka, A. Johansson, and R. Schuch, Nucl. Instrum. Methods Phys. Res. B **258**, 145 (2007).
[16] A. R. Milosavljević, G. Víkor, Z. D. Pešić, P. Kolarž, D. Šević, B. P. Marinković, S. Mátéfi-Tempfli, M. Mátéfi-Tempfli, and L. Piraux, Phys. Rev. A **75**, 030901(R) (2007).
[17] S. Das, B. S. Dassanayake, M. Winkworth, J. L. Baran, N. Stolterfoht, and J. A. Tanis, Phys. Rev. A **76**, 042716 (2007).
[18] T. Ikeda, T. M. Kojima, Y. Iwai, Y. Kanai, T. Kambara, T. Nebiki, T. Narusawa, and Y. Yamazaki, J. Phys.: Conf. Ser. **58**, 68 (2007).
[19] N. Stolterfoht, R. Hellhammer, J. Bundesmann, D. Fink, Y. Kanai, M. Hoshino, T. Kambara, T. Ikeda, and Y. Yamazaki, Phys. Rev. A **76**, 022712 (2007).
[20] R. Hellhammer, J. Bundesmann, D. Fink, and N. Stolterfoht, Nucl. Instrum. Methods Phys. Res. B **258**, 159 (2007).
[21] N. Stolterfoht, R. Hellhammer, D. Fink, B. Sulik, Z. Juhász, E. Bodewits, H. M. Dang, and R. Hoekstra, Nucl. Instrum. Methods Phys. Res. B (to be published).
[22] N. Stolterfoht, R. Hellhammer, J. Bundesmann, and D. Fink, Phys. Rev. A **77**, 032905 (2008).
[23] K. Schiessl, W. Palfinger, C. Lemell, and J. Burgdörfer, Nucl. Instrum. Methods Phys. Res. B **232**, 228 (2005).
[24] K. Schiessl, W. Palfinger, K. Tökesi, H. Nowotny, C. Lemell, and J. Burgdörfer, Phys. Rev. A **72**, 062902 (2005).
[25] P. Skog, H. Q. Zhang, and R. Schuch, Phys. Rev. Lett. **101**, 223202 (2008).
[26] Y. Kanai, M. Hoshino, T. Kambara, T. Ikeda, R. Hellhammer, N. Stolterfoht, and Y. Yamazaki, Phys. Rev. A (to be published).
[27] M. Unipan, A. Robin, D. F. A. Winters, R. Morgenstern, and R. Hoekstra, Phys. Rev. A **74**, 062901 (2006).